# The High-Temperature Work Function of Sintered Dilute Solution Tungsten-Iridium Alloys

*L.A. D'Cruz, D.R. Bosch, and D.L. Jacobson*

**The effect of transition element additives molybdenum, rhenium, iridium, and osmium on the effective work function of tungsten has been the focus of thermionics research for several years.[1-5] In this study, iridium-added tungsten powder mixtures were cold compacted and sintered to produce a range of tungsten-iridium electrodes. An electron emission study was subsequently carried out to evaluate the work function behavior of the consolidated alloys. The work function was obtained from measurements of the current emitted from the electrode surface under ultrahigh vacuum conditions in the temperature range of 1800 to 2500 K using a vacuum emission vehicle (VEV). The data show that the magnitude of the work function in these alloys varied with temperature. Microstructural evaluation of the alloys indicated that the tested surfaces displayed accentuated thermal etching of the grain boundaries together with the fact that the final grain sizes in the sintered alloys were three to five times smaller than those found in equivalent arc-melted alloys that were studied in earlier work.[4,5] Scanning electron microscopy (SEM) micrographs of the tested surfaces of the sintered alloys containing the highest iridium levels (~2 wt%) show a high level of structural distortion, particularly in the vicinity of grain boundaries and corners. The extent of these distortions was found to vary with the iridium content, i.e., the W-IR3M and W-IR2M. The samples with compositions lower than 0.5 wt% Ir were virtually devoid of distortions. It is proposed that, during homogenization carried out prior to testing, a net accumulation of iridium occurs near the surface, particularly in the vicinity of structural heterogeneities. Subsequent cooling leads to the precipitation of iridium-rich second phase sources, which when reheated to the testing temperatures supplies iridium to a surface monolayer. This mechanism is capable of explaining the observed work function trends during high-temperature testing.**

**Keywords:**
high temperature, sintering, tungsten-iridium alloys, work function

## 1. Introduction

THE development of thermionic electrode materials has emphasized the need for substantial improvements in microstructural stability, strength, and creep resistance at service temperatures in excess of 2500 K. This is because future space power operations are characterized by intense energy outputs, which translate into very high operating temperatures for the emitter electrodes in the converter. The addition of small amounts of a transition element has resulted in noticeable trends in work function enhancements (i.e., a higher magnitude of the effective work function of the surface) of tungsten. For example, W-(1%)Ir has been found to result in an effective work function value at 2000 K that is around 7% higher than that exhibited by (110) tungsten.[1] This is considered to be a positive effect from the standpoint of cesiated converter electrode performance. The work function of arc-melted tungsten-iridium alloys was studied in earlier work,[4] wherein it was concluded that a significant depletion of iridium resulted from extended exposure to elevated temperatures. A subsequent study[5,6] found that extended exposure to elevated temperatures resulted in a significant reduction in the work function of the alloys together with a pronounced temperature dependence of the work function. The exact interrelationship between the work function, composition, and geometry of any heated surface is still not fully understood. However, changes in the coverage of an adsorbed surface film have been able to explain the work function variations due to temperature.[7] The film, usually on the order of a few monolayers thick, becomes polarized due to a low of charge between the surface atoms and the substrate surface. In this work, microprobe analyses were carried out on the surfaces of the sintered samples both prior to and following each work function test. The analyses yielded the subsurface iridium compositions of the electrodes and indicated that exposure to elevated temperatures consistently results in lower iridium compositions in the subsurface regions of the electrodes. In this article, an attempt has been made to investigate the interrelationship between the iridium composition and the work function trends in sintered dilute solution tungsten-iridium alloys.

**L.A. D'Cruz, D.R. Bosch,** and **D.L. Jacobson,** Department of Chemical, Bio and Materials Engineering, Arizona State University, Tempe, Arizona.

## 2. Experimental Procedure

### 2.1. *Sample Fabrication*

In this study, a series of tungsten-iridium alloys was fabricated by cold pressing and sintering. Tungsten powder of 99.9% purity and an average particle size of 0.5 μm was used for sample fabrication. Two methods were used for incorporating alloying elements. The first method consisted of mixing weighed quantities of elemental iridium powder (60 μm) with pure tungsten powder (0.5 μm). These powder batches were not subjected to any prereduction procedure. The batches were rotated in a mixing drum under air, and the typical duration of

**Table 1 Iridium compositions determined by electron microprobe analyses of electrodes after sintering and homogenization at 2500 K for 8 to 10 h**

| | Iridium, wt% | | | |
|---|---|---|---|---|
| | Annealed surface | | Ground surface | |
| Sample | Composition, wt% | Grain size, μm | 25 to 50 μm | 50 to 100 μm |
| W-IR0.5C | 0.09 | 84 | 0.02 | 0.16 |
| W-IR1M | 0.00 | ... | 0.03 | 0.35 |
| W-IR2M | 0.37 | 73 | 0.53 | 0.73 |
| W-IR3M | 0.19 | 76 | 0.65 | 0.53 |
| W-IR5M | 1.73 | 77 | 2.19 | 2.65 |

**Table 2 Comparison of iridium compositions before and after vacuum emission vehicle tests on sintered and homogenized electrodes**

| | Iridium composition (a), wt% | | Average grain size, |
|---|---|---|---|
| Sample | Initial | Final | μm |
| W-IR0.5C | 0.16 | 0.01 | 55 |
| W-IR1M | 0.35 | 0.06 | 50 |
| W-IR2M | 0.73 | 0.33 | 56 |
| W-IR3M | 0.53 | 0.30 | 63 |
| W-IR5M | 2.65 | 1.64 | 54 |

(a) Average, measured using electron microprobe on randomly chosen points.

mixing was 20 to 30 min. Mixed batches with iridium additions of 1, 2, 3, and 5 wt% were subsequently cold compacted, sintered, and fabricated into electrodes. These alloys are referred to as the mechanically alloyed samples.

The second processing method consisted of mixing a water-soluble iridium salt solution ($IrCl_3 \cdot 3H_2O$) with the pure tungsten powders to form a slurry that was then dried and treated in a flowing argon/5 vol% $H_2$ gaseous mixture at 1000 K for 24 h to yield an additive-coated tungsten powder. Two batches, containing 0.5 and 1 wt% Ir additions, were prepared by this method. These powders were then cold compacted, sintered, and machined into electrodes. The resulting emitter samples are referred to as the chemically alloyed samples. Cold pressing of the weighed batches of powder was carried out in a hardened tool steel mold at room temperature. The mold walls were precision ground to avoid the use of lubricant during pressing. Compaction of all batches was carried out at a specific load of 45 kN, which corresponded to a compaction pressure of 345 MPa. Batches of 4 g in weight resulted in cylindrical samples with diameter of 1.27 cm and 0.32 cm thick (i.e., 1/2 × 1/8 in). These samples possessed green densities in the range of 40 to 45% of theoretical.

An electron bombardment heated bell-jar furnace was used to sinter the samples in vacuum. A vacuum of around $5 \times 10^{-6}$ torr was consistently maintained during operation of the furnace. Temperature was measured by a W-3Re/W-25Re thermocouple. The compacts were initially subjected to isothermal 1 h heat treatments at 1492 and 1700 K. This procedure was found to reduce sagging in the compact during high-temperature sintering. The final step of sintering was carried out at approximately 2200 K for a total of 4 h. The resultant compacts were found to have bulk densities near 95% of theoretical. The fabricated alloys were designated W-IR1M, W-IR2M, W-IR3M, W-IR5M, W-IR0.5C, and W-IR1C. The final letter of the designation code indicates the alloying procedure used, namely M for mechanical alloying and C for chemical alloying. The number used in the code corresponds to the intended amount of iridium added during powder processing. There were, however, iridium losses associated with mixing and handling as well as losses due to the evolution of gaseous iridium oxides. The formation and evolution of gaseous oxides is likely to be restricted to the lower temperatures in the sintering procedure because the iridium oxides ($IrO_2$ and IrO) are unstable at temperatures above 1200 K. As a result of these losses, the final composition of the consolidated electrode is different from the intended amount added during processing. The actual compositions were obtained by electron probe microanalyses of the polished surfaces of the consolidated compacts that were homogenized for 8 to 10 h at 2500 K under ultrahigh vacuum. These compositions are presented in the last column of Table 1. Because these composition values were obtained after grinding off about 100 μm of the surface, they have been taken to be the initial iridium content of the electrode, and are presented in Table 2.

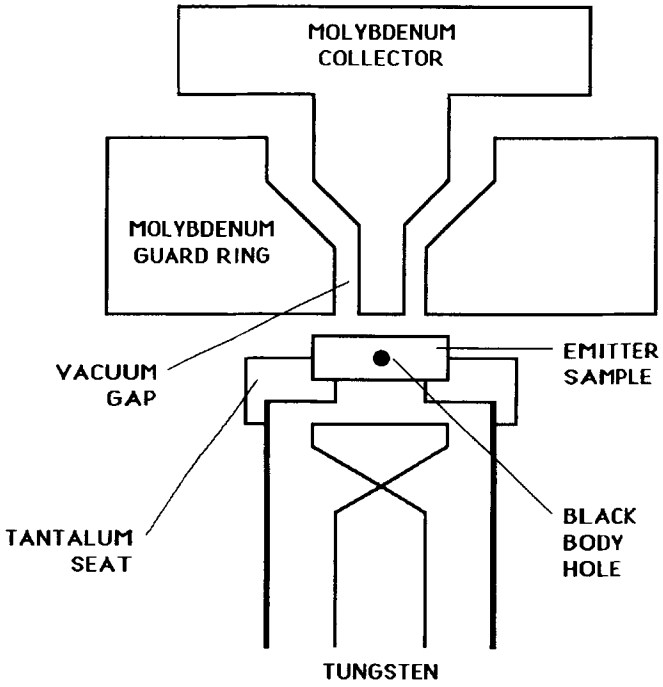


**Fig. 1** Schematic of the vacuum emission vehicle.[4]

**Table 3 Effective work functions from pilot tests on as-fabricated tungsten-iridium alloys**

| Temperature, K | Work functions, eV | | | | | |
|---|---|---|---|---|---|---|
| | W-IR0.5C | W-IR1M | W-IR2M | W-IR3M | W-IR5M | W-IR1C |
| 1800 | 4.83 | 4.87 | 4.83 | 4.71 | 5.04 | |
| 1900 | 4.85 | 4.92 | 4.91 | 4.83 | 5.04 | 5.04 |
| 2000 | 4.84 | 4.91 | 4.92 | 4.85 | 5.00 | 5.01 |
| 2100 | 4.80 | 4.88 | 4.89 | 4.85 | 4.99 | 4.93 |
| 2200 | 4.75 | 4.82 | 4.90 | 4.88 | 4.98 | 4.90 |
| 2300 | 4.69 | 4.78 | 4.84 | 4.84 | 4.95 | 4.86 |
| 2400 | 4.66 | 4.74 | 4.81 | 4.83 | 4.95 | 4.82 |
| 2500 | 4.63 | 4.69 | 4.75 | 4.76 | 4.88 | 4.80 |

**Table 4 Effective work functions of sintered and homogenized tungsten-iridium alloys**

| Temperature, K | Work functions, eV | | | | |
|---|---|---|---|---|---|
| | W-IR0.5C | W-IR1M | W-IR2M | W-IR3M | W-IR5M |
| 1800 | 4.90 | 4.73 (4.79) **(a)** | 4.83 (4.81) **(a)** | 4.70 (4.83)**(a)** (4.69)**(b)** | 4.67 (4.91) **(a)** |
| 1900 | 4.90 | 4.88 (4.93) **(a)** | 4.94 | 4.83 | 4.84 |
| 2000 | 4.86 | 4.93 | 4.93 (4.95) **(a)** | 4.90 | 4.94 (5.05) **(a)** |
| 2100 | 4.82 | 4.89 | 4.91 | 4.90 | 4.97 |
| 2200 | 4.76 | 4.83 | 4.86 (4.88) **(a)** | 4.81 | 4.95 (4.97) **(a)** |
| 2300 | 4.75 | 4.78 | 4.84 | 4.78 | 4.96 |
| 2400 | 4.70 | 4.72 | 4.81 | 4.73 | 4.93 |
| 2500 | 4.65 | 4.70 | 4.75 | 4.67 | 4.88 |

**(a)** Obtained on second run sequence immediately after completion of primary 1800 to 2500 K sequence. **(b)** Obtained after cooling and reheating to temperature.

### 2.2. *Work Function Evaluation*

Work functions were determined at high temperatures (1800 to 2500 K) with a guard-ringed vacuum emission vehicle (VEV) using the thermionic method. The basic design of the vacuum emission vehicle is illustrated in Fig. 1. A detailed description of the setup has been presented elsewhere.[8,9] Each sample was ground and polished with fine alumina (0.05 μ) powder. The polished sample was mounted in the vacuum emission vehicle as the emitter, following which the chamber was evacuated and baked to attain a vacuum of $3 \times 10^{-10}$ torr. The sample was then heated to 2500 K and annealed insitu for 8 to 10 h, after which the sample was cooled to room temperature without loss in vacuum. The current measurement device (Kiethley 610C Electrometer) was connected through the external ultrahigh vacuum feedthroughs of the chamber, and an electric field was applied between the emitter and the collector (Fig. 1). The sample was then heated by electron bombardment to the first experimental temperature, i.e., 1800 K. The emission current from the sample surface was measured using a Kiethley 610C Electrometer, and the temperature of the sample was measured using a disappearing-filament pyrometer focused on a hohlraum machined into the side face of the sample disc.

The effective work function was then calculated by an online computer using a combination of the Richardson-Dushman equation and the Shottky equation.[8,9] The uncertainty in the effective work function obtained by this system has been determined to be 0.04 eV.[3] Data collection at each temperature was carried out for 15 to 20 min to provide an average value for the effective work function at that temperature. The sample was then heated to the next temperature (in increments of 100 K) where the same data collection procedure was repeated. The maximum experimental temperature studied during this work was 2500 K.

## 3. Results and Discussion

### 3.1. *Pilot Tests on Consolidated Alloys*

A preliminary test (pilot test) was run on each of the as-fabricated electrodes. The purpose was twofold, the first being to carry out the self-cleaning and homogenization of the electrode, and the second was to obtain a preliminary estimate of the work function trends. A heat treatment procedure consisting of annealing at 2500 K for 8 to 10 h followed by cooling to room temperature was typically used immediately prior to testing of each vacuum emission vehicle electrode. Data corresponding to the pilot tests are presented in Table 3. Following the pilot tests, the average iridium composition was obtained by performing electron probe microanalysis on the emitter surface of the electrodes. Scanning electron microscopy (SEM) was also used to investigate the topography of the surface. The tested surface of the electrode was then ground off and polished to remove approximately 25 μm of material, following which electron probe microanalysis was again carried out on the surface. This measurement corresponded to the bulk composition at a depth of approximately 25 μm below the original tested surface. The sequence of grinding, polishing, and microanalysis was repeated once again to measure the composition at an even greater depth (100 μm) from the original surface. The iridium concentration so obtained was taken to be the initial irid-

ium content of the alloys, i.e., prior to the work function evaluation of the alloys.

### 3.2. *Effective Work Function versus Temperature*

The homogenized and resurfaced samples were tested using the work function evaluation procedure described earlier to obtain the effective work function as a function of temperature. The work function values corresponding to each alloy in the temperature range of interest are presented in Table 4. Figure 2 shows the variation in work function with the temperature for each of the alloys. Some of the alloys were subjected to a second measurement cycle that was commenced at 1800 K immediately after data collection for the highest temperature (i.e., at 2500 K) was completed. This was accomplished by immediately lowering the temperature to 1800 K and repeating the data collection sequence. These work functions are presented in parentheses alongside the values obtained in the first cycle (Table 4).

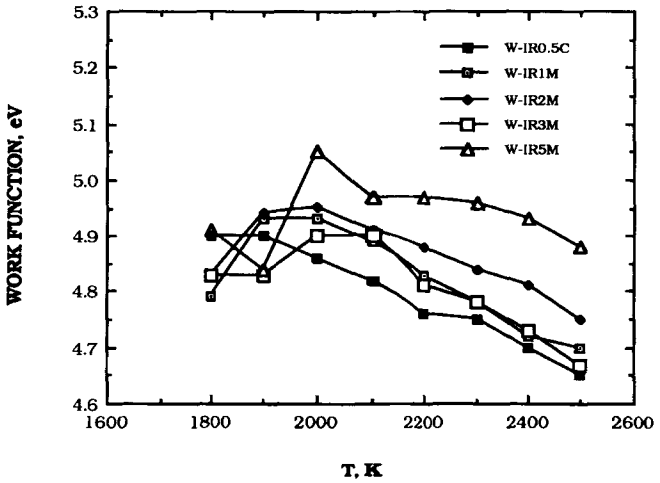


**Fig. 2** Effective work function of tungsten-iridium alloys as functions of temperature and iridium content.

The following general trends emerge from the data obtained for the sintered alloys. For each alloy, the plots of the work function versus temperature exhibited a work function maximum, at a temperature between 1900 and 2100 K. For higher iridium contents, the maximum seemed to occur at a higher temperature (Table 4). The effective work function decreased significantly with temperature after a maximum value had been attained. The gradient of the decrease appeared to be smaller for samples with higher iridium contents (see Fig. 2). The work function exhibited a hysteresis effect at lower temperatures. At any particularly experimental temperature, a higher value of the effective work function was obtained when the sample was cooled to that temperature from a higher temperature (values in parentheses in Table 4) than the value obtained during sequential heating from lower temperatures. This effect tended to be more pronounced for higher iridium contents.

With the electrode surfaces essentially unaltered after the first set of experimental tests and characterization, selected samples (W-IR3M and W-IR5M) were reintroduced into the chamber and retested following the identical procedure used earlier. The motivation of the repeated tests was to investigate the reproducibility of the data obtained in the first test. The data obtained during the second test are compared with that from the first test in Fig. 3(a) and (b). It can be seen that the work functions obtained in the second test were significantly higher than those corresponding to the first test over most of the temperature range. It is interesting to note that the arc melted alloys studied in an earlier work[4,5] exhibited the exact opposite trend, i.e., the second test yielded work functions that were significantly lower in magnitude than those of the first test. These observations provide an insight into the interrelationship between extended heating and temperature cycling, the work function values, and the compositional changes near the surface of the dilute solution tungsten-iridium electrode.

Burton and Machlin[10] reported that a solute that forms a eutectic with the solvent would segregate to the surface of the solid solvent in a high vacuum. They suggested that the same sources that tend to expel the solute from the solid phase to the

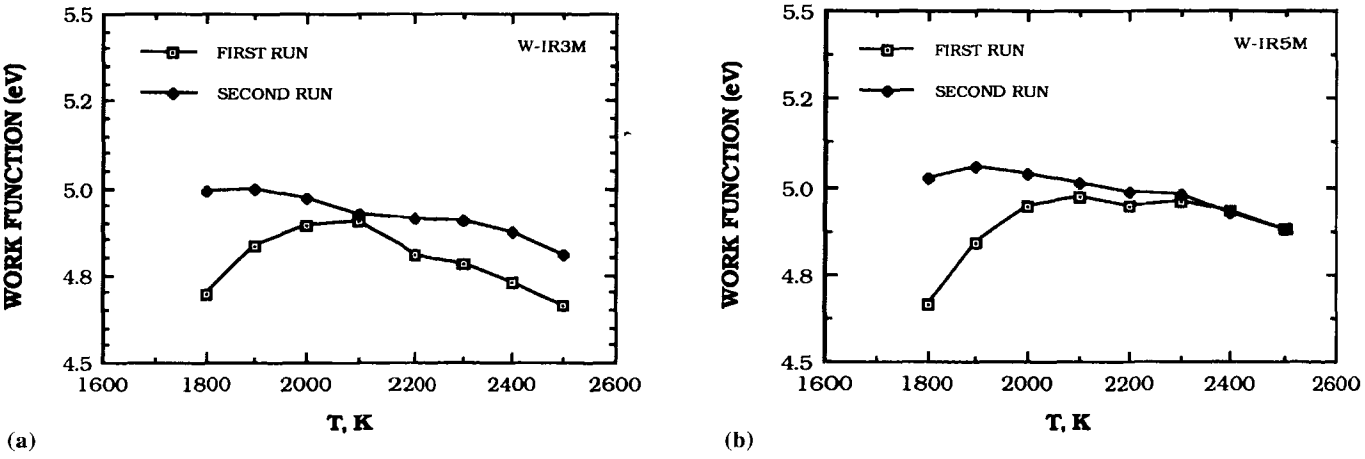


**Fig. 3** Variation of effective work function with temperature during second vacuum emission vehicle test. **(a)** W-IR3M. **(b)** W-IR5M.

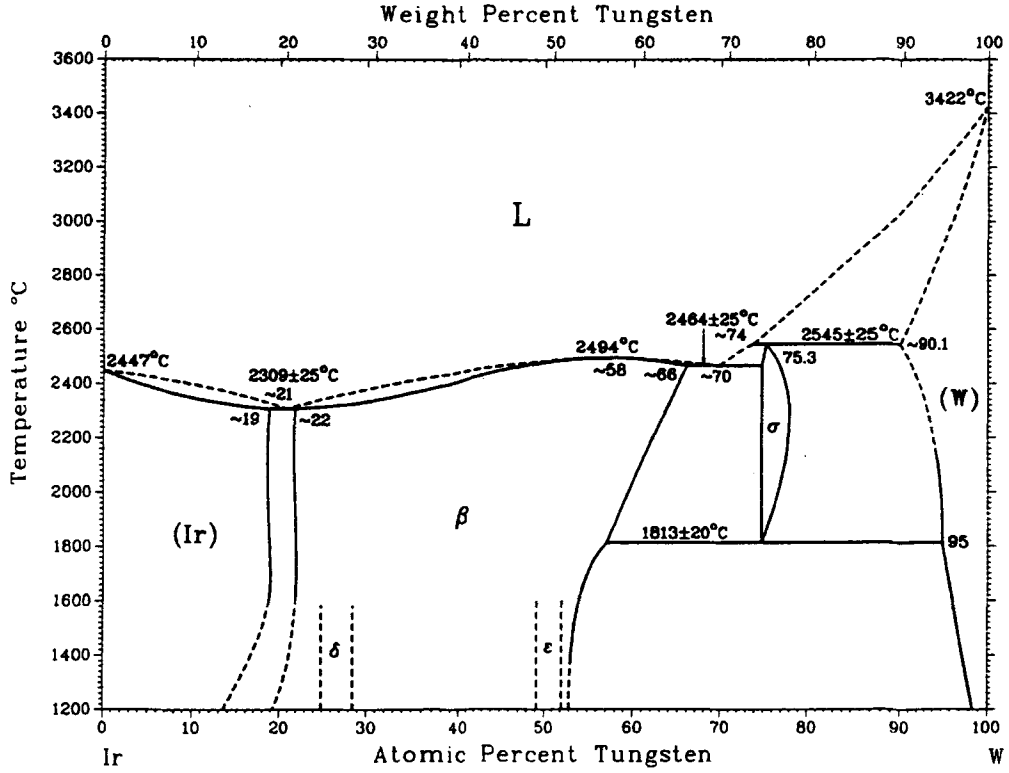


**Ir-W crystal structure data**

| Phase | Composition, at.% W | Pearson symbol | Space group | Strukturbericht designation | Prototype |
|---|---|---|---|---|---|
| (Ir) | 0 to 19 | *cF*4 | $Fm\bar{3}m$ | *A*1 | Cu |
| β | ~22 to 66 | *hP*2 | $P6_3/mmc$ | *A*3 | Mg |
| δ | ~25 | *hP*8 | $P6_3/mmc$ | $D0_{19}$ | $Ni_3Sn$ |
| ε | ~50 | *oP*4 | *Pmma* | *B*19 | AuCd |
| σ | ~75 | *tP*30 | $P4_2/mnm$ | $D8_b$ | σCrFe |
| (W) | ~90 to 100 | *cI*2 | $Im\bar{3}m$ | *A*2 | W |

**Fig. 4** Tungsten-iridium equilibrium phase diagram.[12]

liquid phase during solidification would set up the migration of the solute atoms from the solid phase to its free surface. The equilibrium phase diagram of the tungsten-iridium system (Fig. 4) does in fact exhibit two eutectic transformations. This implies that the migration of iridium to grain boundaries and the surface could occur in the alloys studied in this work. Luo[11] has reported that, in dilute solution tungsten-iridium alloys, the transition from transgranular fracture to intergranular fracture occurred at a lower temperature in a W-0.8 wt% Ir alloy compared to a W-0.4 wt% Ir alloy. This fact has been attributed to the segregation tendency of iridium in tungsten.

The topographical evolution of the electrode surfaces as well as the observed compositional changes of the subsurface layers could explain the lack of reproducibility in the effective work function values yielded by successive tests. The decomposition of iridium-saturated surface layers into iridium-rich metastable phase(s) during cooling from high temperature to room temperature at the end of the test appears to be consistent with the phase diagram (Fig. 4). Such an accumulation of iridium at the surface could account for the sharp rise in work function obtained during the second test carried out on the sintered samples with higher bulk iridium levels. The hysteresis effect described earlier (see values in parentheses in Table 4), where the work function increased during the first test when the temperature was lowered from 2500 to 1900 K, is also consistent with this possibility. In the event that a net accumulation of iridium does occur at the surface, it would be governed by a balance between two dynamic processes operating at the surface, namely, the iridium flux diffusing to the topmost layers of the surface from the interior and the flux leaving the surface by sublimation.

The arc-melted alloys display work function trends[4,5] that were exactly the opposite of those found in the sintered alloys. Retesting the samples in the current study resulted in a lower work function over the entire temperature range. A possible explanation for this trend is that the extent of surface enrichment

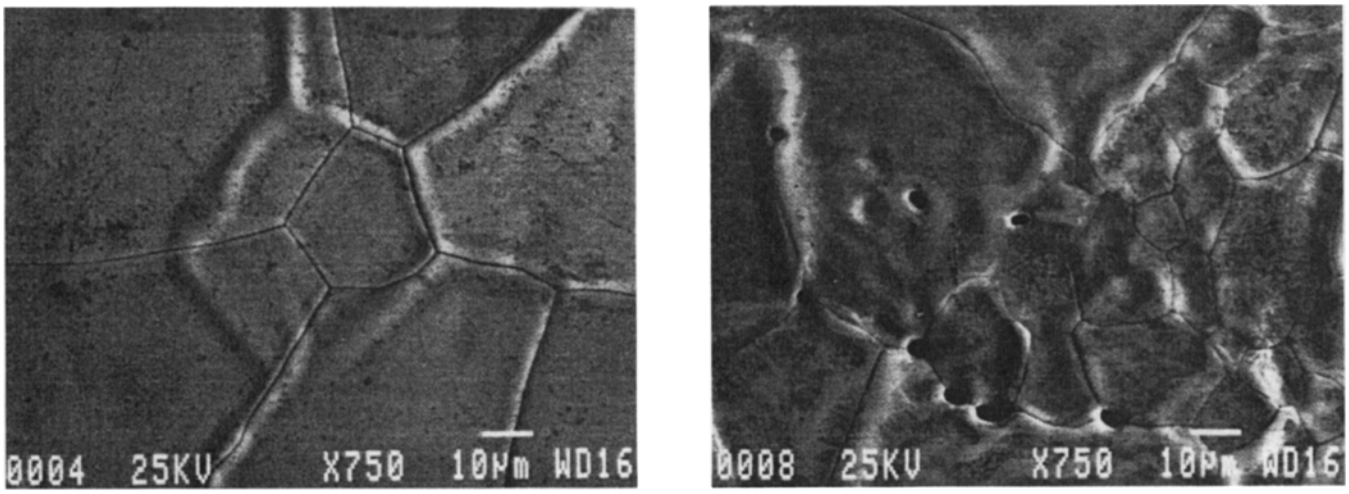


**Fig. 5** SEM micrographs of electrode surfaces after pilot tests. **(a)** W-IR0.5M. **(b)** W-IR2M.

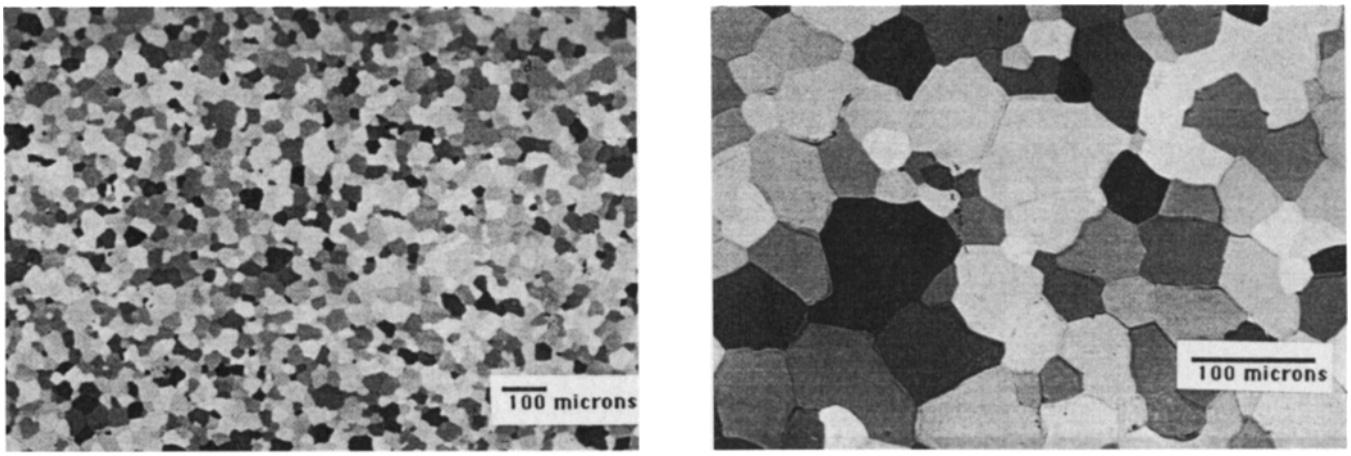


(a) (b)

**Fig. 6** Backscattered electron micrographs of the surface of the W-IR1M sample produced by post-homogenization vacuum emission vehicle tests.

in the arc-melted alloys was significantly lower. This may be because the arc-melted alloys possessed insufficient fast diffusion paths to the surface due to the large grain sizes. Also, the smoother surface topography of these alloys could result in a high rate of sublimation of surface atoms.

### 3.3. *Microstructural Evaluation*

Following the completion of each work function evaluation, the sample was cooled to room temperature and extracted from the vacuum emission vehicle chamber for microstructural and compositional analysis. Scanning electron microscopy performed immediately after the homogenization/pilot test revealed that the sample surfaces were dense, but significantly distorted probably due to the shrinkage of residual pores (Fig. 5). As described earlier, these surfaces were then subjected to repeated sequences of grinding, polishing, and electron probe microanalysis. The results of the compositional analysis carried out after the completion of homogenization as well as compositions obtained after each grinding sequence are presented in Table 1. The compositions, measured after the regular work function testing, are presented in Table 2. Compositional backscattered electron (BSE) images of the tested surfaces are shown in Fig. 6 and 7, verifying therefore that this procedure resulted in a uniform, well-defined microstructure with uniform grain sizes. The alloys with higher iridium contents, however, exhibited less sharpness in the vicinity of the thermally etched grain boundaries. These distortions show up

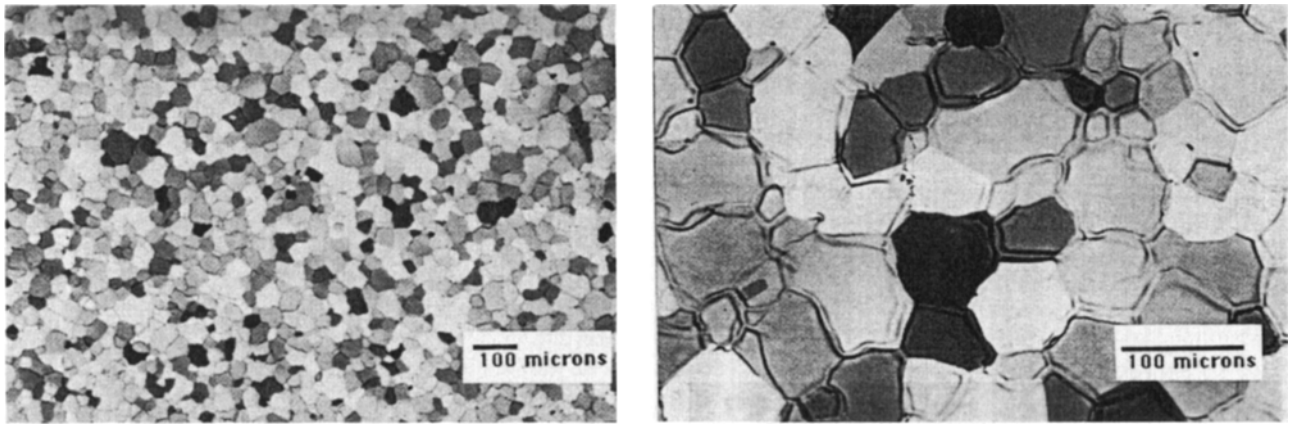


**Fig. 7** Backscattered electron micrographs of the surface of the W-IR5M sample produced by post-homogenization vacuum emission vehicle tests.

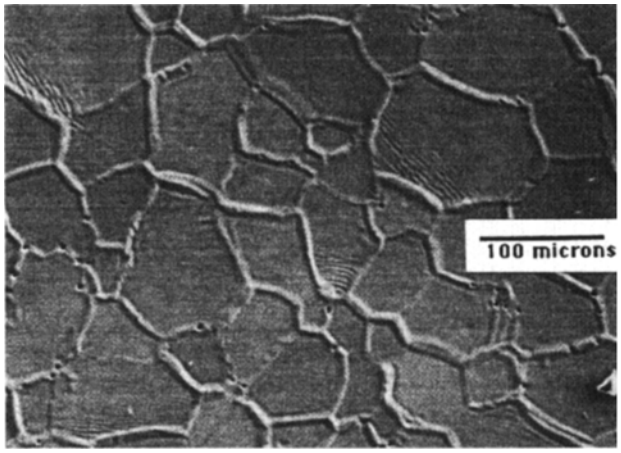


**Fig. 8** SEM micrograph showing the topography of the W-IR3M sample surface after extended testing.

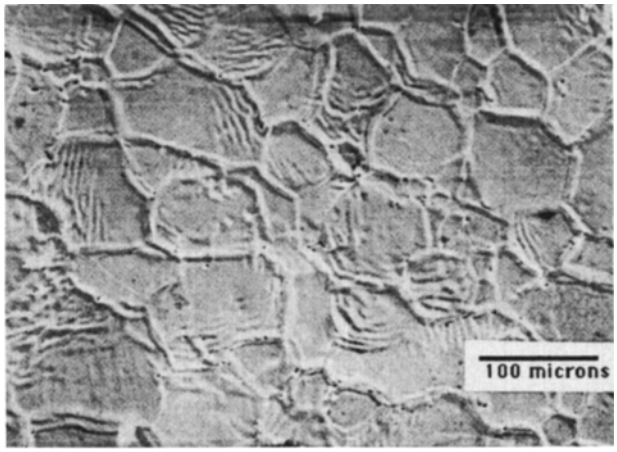


**Fig. 9** SEM micrograph showing the topography of the W-IR5M sample surface after extended testing.

clearly in the secondary electron images shown in Fig. 8 and 9. The topography of the distortion seems to indicate that the processes that formed them were associated with dislocation defects extending from the grain boundaries.

The fact that the topography is more intense in the high-iridium sample indicates a strong interaction between the defects and iridium atoms. Because the iridium atomic radius is approximately 7.5% smaller than that of the tungsten atom, it is reasonable to expect that iridium would stabilize dislocations in the vicinity of the grain boundary by relieving the defect strain. When the iridium concentration is low, the dislocations are less influenced by the iridium content and are eventually annealed out of the microstructure. It is reasonable to expect that the stabilized dislocations, while participating in creep processes at elevated temperatures (1900 to 2500 K), would alter the iridium arrival rate at the surface. Iridium migration characteristics are influenced by the fact that the dislocations, in moving toward the surface and grain surfaces, would supply iridium atoms to these locations. This would be manifested as a decrease in the activation energy of diffusion of iridium to the surface. In this manner, the creation of an iridium monolayer on the electrode surface could be governed to a greater degree by the energetics of fast diffusion via defects rather than volume diffusion.

One important point needs to be made here, which further complicates the picture just described. Even though tungsten is self-cleaning, oxygen at the surfaces of the initial tungsten powders is not removed completely during vacuum sintering. The entrapped oxygen competes for grain boundary and defect sites and hence affects the iridium transport through these paths. It is also possible that strong chemical interactions between iridium, tungsten, and oxygen atoms would take place near the grain boundaries, which in turn would affect the transport of both iridium and oxygen to the surface. Also noteworthy is the fact that $Ir_2O_3$ is a thermodynamically stable liquid up to 2250 K.[13] In the event that the iridium oxide forms and is transported to the surface, it would modify the work function of the surface. One possible reaction that is likely to occur at

surfaces exposed to vacuum is decomposition of the oxide accompanied by iridium deposition in surface regions along with the evolution of tungsten oxide or gaseous oxygen. The occurrence of such a chemical reaction could explain the considerable instability exhibited by the work function curves shown in Fig. 2 at temperatures between 1800 to 2200 K, especially in the case of higher iridium contents. The work function plots of the W-IR0.5C alloy did not display such fluctuations. It should be pointed out that unlike the rest of the samples, the W-IR0.5C sample was sintered under reducing conditions, and its homogenized microstructure was extremely uniform (Fig. 5a).

This discussion has provided two separate mechanisms for the formation of an iridium layer on the surface of tungsten at elevated temperatures. One involves the interaction of iridium with defects in tungsten near the grain boundaries, and the other involves the interaction of iridium with oxygen at the grain boundaries. Secondary ion mass spectroscopy (SIMS) images and transmission electron microscopy (TEM) have been performed on the surfaces of the electrodes with the highest iridium content (W-IR5M) and presented elsewhere.[6,14] These initial results have indicated regions of iridium accumulation together with what appears to be disc-shaped second phase particles and regions with lamellar morphology.

## 4. Summary and Conclusions

The work function obtained for a series of sintered dilute solution tungsten-iridium alloys was studied with the primary intention of evaluating the effect of iridium composition. The powder compaction-vacuum sintering route used for processing the alloys was associated with significant iridium losses. This resulted primarily due to reaction with residual oxygen in the sintering vacuum chamber and to some extent due to sublimation. Nevertheless, the work function evaluation of the fabricated and annealed alloys, which was performed under ultrahigh vacuum, indicated that the magnitude of the effective work function was related to the subsurface compositions measured immediately prior to the test. The highest composition of 2.65 wt% Ir (measured in the W-IR5M sample) corresponded to the highest work function at all temperatures in the range of testing. Post-test compositional analysis indicated a significant reduction in the subsurface composition for all alloys tested. The magnitude of the composition change caused by elevated temperature testing appeared to increase linearly with the initial composition of the electrode. The repeatability of the work function was evaluated with the help of pilot test data obtained immediately after fabrication of the alloys (but prior to the regular work function tests wherein the samples were ground, polished, and tested to obtain the effective work function versus temperature data presented in this work).

Comparison of the two tests indicates that the repeatability is good only for lower iridium compositions (<0.5 wt%). Further testing of the samples containing higher levels of iridium resulted in higher work functions over the entire temperature range. These observations are clearly indicative of a net increase in iridium atom concentration on the surface of the electrode in the retested samples. This may be due to the formation of an iridium monolayer film probably due to the high-temperature anneal and subsequent quenching to room temperature, which preceded every test. Changes in the work function of a surface are often interpreted in terms of changes in the coverage of a dipole layer on the surface, which becomes polarized due to the flow of charge between the surface atoms and the substrate surface.[7] The observations reported in this article lend support to the hypothesis that an iridium monolayer forms on the electrode surfaces, thus modifying the effective work function. The variation in effective work function with temperature depends on the balance between the flux associated with sublimation of iridium atoms from the surface and the diffusion flux arriving at the surface in the temperature range of testing.

## Acknowledgments

This work was funded by the Wright Research and Development Center, WPAPL, Ohio, under contract No. F-33615-87-C-2769, Arizona State University. The authors would like to thank Mr. Jim Clark at the Electron Microprobe Lab, Department of Chemistry, for assistance with the compositional analysis. The JEOL JXA-8600 electron microprobe was purchased with the aid of NSF grant EAR-8408163.

### References

1. D.L. Jacobson, *Metall. Trans*, Vol 3, 1972, p 1263
2. M.L. Ramalingam, S. Snir, and D.L. Jacobson, *J. Mater. Eng.*, Vol 9, 1988, p 353
3. N.O. Moraga, Ph.D dissertation, Arizona State University, 1988
4. R. Wall and D.L. Jacobson, *High-Temp. Sci.*, Vol 30, 1991, p 95
5. L.A. D'Cruz, D.R. Bosch, and D.L. Jacobson, *High-Temp. Sci.*, to be published
6. L.A. D'Cruz, Ph.D dissertation, Arizona State University, 1991
7. E.P. Gyftopoulos and J.D. Levine, *J. Appl. Phys.*, Vol 33, 1962, p 67
8. D.L. Jacobson and A.E. Campbell, *Metall. Trans.*, Vol 2, 1971, p 3063
9. R.N. Wall and D.L. Jacobson, *J. Mater. Eng.*, Vol 11, 1989, p 197
10. J.J. Burton and E.S. Machlin, *Phys. Rev. Lett.*, Vol 37, 1976, p 1433
11. A. Luo, K.S. Shin, and D.L. Jacobson, *Scri. Metall. Mater.*, Vol 25, 1991, p 2411
12. *Binary Alloy Phase Diagrams*, T.B. Massalski, Ed., ASM International, 1990, p 2368
13. *The Oxide Handbook*, G.V. Samsonov, Ed., IFI/Plenum, New York, 1982 (translated from Russian)
14. L.A. D'Cruz, D.R. Bosch, and D.L. Jacobson, *J. Refract. Met. Hard Mater.*, to be published